INSTITUTE OF PHYSICS PUBLISHING JOURNAL OF PHYSICS B: ATOMIC, MOLECULAR AND OPTICAL PHYSICS

J. Phys. B: At. Mol. Opt. Phys. **39** (2006) 2493–2503 doi:10.1088/0953-4075/39/11/014

The resonance structures in the cross sections of slow electron interaction with barium atoms: a fully relativistic *R*-matrix study

Jianhua Wu and Jianmin Yuan

Department of Physics, National University of Defense Technology, Changsha 410073, People's Republic of China

Received 5 January 2006, in final form 30 March 2006
Published 15 May 2006
Online at stacks.iop.org/JPhysB/39/2493

Abstract

A 23-state close-coupling calculation on the slow electron interaction with barium atoms is carried out by using a fully relativistic *R*-matrix method. The results for the slow electron scattering and photodetachment of the negative atomic barium ions are presented. An apparent relativistic fine-structure split is produced for both the bound states of the negative ion and the shape resonance states of the free electron. The electron affinities for the $6s^2 6p\ ^2P^o_{3/2}$ level and the $6s^2 6p\ ^2P^o_{1/2}$ level are obtained to be 183 meV and 240 meV, respectively. The 57 meV fine-structure split of the 6p orbital is very close to the experimental value. The fine-structure split of the d-wave shape resonance above the elastic threshold is predicted to be 31 meV. The calculated integral scattering cross sections from 0 to 10 eV show that including the relativistic effects cannot eliminate the large discrepancies between theory and the existing experiment.

1. Introduction

Low-energy electron interaction with alkaline-earth atoms has been extensively studied in the past decade. The interest in the study of the electron scattering with alkaline-earth atoms and the photodetachment of their negative ions was stimulated by the fact that Ca and other heavier alkaline-earth atoms can form stable negative ions [1, 2] by absorbing an extra electron outside a closed shell. These studies include the binding energies of the negative ions [3–16], low-energy electron collisions with alkaline-earth atoms [17–30] and the photodetachment of the very loosely bound alkaline-earth negative ions [31–38]. Among these studies, only a few of them were concerned with the low-energy electron interaction process with barium atoms. The only measurement for the absolute scattering cross sections of a low-energy electron from barium atoms below 10 eV was taken by Romanyuk *et al* [19]. Even for theoretical studies, calculations about the interaction between a slow electron and barium atoms are not quite popular either, due to the complexity of the calculations caused by both the correlation and

relativistic effects. A limited close-coupling calculation was given by Fabrikant [17]. Gribakin *et al* [35] carried out a calculation in which the bound state wavefunction of the negative ion was obtained by solving the non-relativistic Dyson equation to include the correlation effect, and the accuracy of the theory was, however, weakened by using a Hartree–Fock approximation to describe the continuum wavefunction of the free electron. A non-relativistic close-coupling calculation was given by one of the present authors [39] by using the R-matrix method with 21 states being included in the close-coupling expansion, and part of the core–valence correlation was considered as well.

By using a comprehensive close-coupling approach, reasonably good agreement between theory and experiment can be obtained for both slow electron scattering cross sections and the photodetachment cross sections for all the atoms before barium [22, 37–39]. However, the total cross section of electron scattering from barium atoms was predicted by the theoretical calculations [39] as being almost twice that of the experimental values when the free electron energy is above 2 eV. The relativistic effect was suspected to be responsible for such large discrepancies between theory and experiment. To the best of our knowledge, however, there is no comprehensive, fully relativistic close-coupling calculation for the interaction of slow electrons with barium atoms so far. In the present study, the fine-structure split of the shape resonance states, the near-threshold structure of the photodetachment cross sections of negative atomic barium ions and the slow electron scattering cross section from barium atoms will be focused on by carrying out a fully relativistic 23-state close-coupling calculation with the relativistic R-matrix approach.

2. Theoretical methods

The R-matrix method for electron–atom and photon–atom interactions has been discussed in great detail by Burke *et al* [40]. The present calculations have been carried out by using the fully relativistic R-matrix code DARC [41, 42]. We will just give an outline as follows.

In an R-matrix calculation, the wavefunction of the $N + 1$ electron system is given by the form

$$\Psi_k(X_1 \dots X_{N+1}) = \hat{A} \sum_{ij} c_{ijk} \Phi_i(X_1 \dots X_N \hat{r}_{N+1} \sigma_{N+1}) \times u_{ij}(r_{N+1}) + \sum_j d_{jk} \phi_j(X_1 \dots X_{N+1}), \tag{1}$$

where $\hat{A}$ is the antisymmetrization operator to take the exchange effect between the target electrons and the free electron into account. X_i stands for the spatial (r_i) and the spin (σ_i) coordinates of the ith electron. The functions $u_{ij}(r)$ under the first sum construct the basis sets for the continuum wavefunctions of the free electron. For each angular momentum, they are normally obtained by solving the model single-channel scattering problem and are orthogonal both to themselves and to the bound orbitals. The bound orbitals plus the continuum orbitals then form a larger size of basis set for the $N + 1$ electron system than for the N electron target states. Φ_i is the coupling between the target wavefunction of a specific level $J_i\pi_i$ and the angular and spin part of the free electron. The target states are usually written as a configuration–interaction (CI) expansion in terms of some basis configurations, which are constructed from a bound orbital basis set consisting of self-consistent field orbitals plus some additional pseudo-orbitals included to model electron correlation. The correlation functions ϕ_j in the second sum are formed from the same set of bound orbitals and must be included to compensate for the incompleteness of the continuum orbitals. They can also be used to compensate for the correlation effects not adequately considered because of the cut-off in the first sum.

Table 1. Calculated energy levels (in eV) of the first 20 low-lying excited states of Ba compared with experimental results [44].

Configuration	Term	J	Theory	Experiment
$6s^2$	^1S	0	0.0	0.0000
6s5d	^3D	1	1.112	1.120
		2	1.130	1.142
		3	1.161	1.190
6s5d	^1D	2	1.430	1.413
6s6p	$^3P^o$	0	1.309	1.512
		1	1.358	1.568
		2	1.469	1.676
6s6p	$^1P^o$	1	2.141	2.239
$5d^2$	^3F	2	2.472	
		3	2.493	
		4	2.521	
5d6p	$^1D^o$	2	2.641	2.861
5d6p	$^3F^o$	2	2.548	2.736
		3	2.663	2.845
		4	2.743	2.945
$5d^2$	^1D	2	2.833	2.859
$5d^2$	^3P	0	2.820	2.878
		1	2.847	2.911
		2	2.905	2.966

In the relativistic R-matrix calculations, the orbitals are obtained from multiconfigurational Dirac–Fock code GRASP [43] by using an extended average level (EAL) optimizing process for the concerned energy levels of the neutral atom included in the close-coupling expansion. The single particle functions have the form

$$\varphi(r) = \frac{1}{r}\begin{pmatrix} P_{n\kappa}(r)\chi_{\kappa}^{m}(\theta,\phi) \\ i\,Q_{n\kappa}(r)\chi_{-\kappa}^{m}(\theta,\phi) \end{pmatrix} \tag{2}$$

where $P_{n\kappa}(r)$ and $Q_{n\kappa}(r)$ are respectively the large and small component radial wavefunctions, and the functions $\chi_{\pm\kappa}^{m}(\theta,\phi)$ are two-component spinors made up of spherical harmonics and Clebsch–Gordan coefficients. The radial parts of the bound orbitals are input to the fully relativistic R-matrix code as numerical values on a suitable mesh of points.

In the present calculations, the barium atom target wavefunctions are described by a closed core $1s^22s^22p^63s^23p^63d^{10}4s^24p^64d^{10}5s^25p^6$ and eight valence one-electron orbitals obtained by using the EAL optimizing process. The valence orbitals are $5d_{3/2}$, $5d_{5/2}$, $6s_{1/2}$, $6p_{1/2}$, $6p_{3/2}$, $6d_{3/2}$, $6d_{5/2}$, and $7s_{1/2}$, and interactions between the configurations generated by all possible excitations of the two 6s electrons among all the valence orbitals are considered. The 23 lowest levels are included in the expansion of the wavefunction in performing the relativistic R-matrix calculation. The first 20 theoretical energy levels are given in table 1 along with the experimental results [44]. Though our results agree with the experimental results fairly well, some differences still exist. Firstly, most of the calculated energy levels are slightly lower than the experimental values. We attribute this discrepancy to the not-included core–valence electron correlation in the present calculations. For heavy alkaline-like atoms, core–valence correlation was found to be important in the photodetachment process in previous works [12, 39]. Including the core–valence correlation can lower the ground state of the atom [39], thus the relative energy levels might be closer to the experimental data.

However, it would be a really big calculation if the core–valence correlation was included. In the present relativistic calculation, we placed the emphasis on the fine-structure split and the influence on the slow electron scattering cross section caused by the relativistic effects, so the core–valence correlation was ignored as long as fairly good energy levels were obtained. Secondly, there are no experimental data for the energy levels of $5d^2\ ^3F_{2,3,4}$, while they are given in the present theoretical calculation. In the present results these levels are lower than that of $5d^2\ ^1D_2$, and that is consistent with Hund's rule. More precise experimental results are required to verify our results. According to the biggest convergence radius of the single electron orbital wavefunctions, the R-matrix boundary was chosen to be 60 au in the present calculation to ensure the wavefunction was completely wrapped within the R-matrix sphere.

3. Results and discussions

The accuracy of both the initial and final states is quite essential for the description of the photodetachment process. The same set of bound electron orbitals is used for both the neutral atom and the negative ion, which are obtained with the EAL optimizing facility for the energy levels of the neutral target. This set of the bound state orbitals is far from sufficient for the description of the very loosely bound states of the absorbed electron in the negative ion. Nevertheless, this less extension of the one-electron orbitals is improved effectively by the algorithm of the R-matrix scheme for the bound states. This is achieved by connecting the wavefunctions of the $N + 1$ electron given by equation (1) inside the R-matrix sphere smoothly with an exponentially decaying wavefunction outside the sphere at the boundary. In the internal region, the continuum orbitals, obtained by solving the model single-channel scattering problem, are orthogonal both to themselves and to the bound orbitals. The bound orbitals plus the continuum orbitals then form a larger basis set of functions compared with the basis set for the N electron target system over the internal region. The inclusion of the continuum orbitals for the $N + 1$ electron system is also helpful in avoiding the possible overestimation of the coupling between the neutral and the negative ion states when the same set of bound orbitals is used for both of them. Electron affinities of 183 meV for $Ba^-6s^26p\ ^2P_{3/2}$ and 240 meV for $Ba^-6s^26p\ ^2P_{1/2}$ are obtained in the present relativistic close-coupling calculation. These bound energies are very close to 192 meV of a valence-only calculation [5] and the only other two non-relativistic R-matrix approach results of 176 meV [4] and 183 meV [39]. However, the given experimental electron affinities [16] of $Ba^-6s^26p\ ^2P_{3/2}$ and $Ba^-6s^26p\ ^2P_{1/2}$ are 89.60 ± 0.06 and 144.62 ± 0.06 meV respectively, much smaller than the present calculated results. As many other authors [12, 39] have discussed before, including core–valence correlation for alkaline-earth atoms will lead to considerable reduction of the electron affinity. For the reasons we discussed above, the core–valence correlation was neglected in the present calculation as we had obtained reasonably good low-lying energy levels of the barium atom. Nevertheless, the fine-structure split, which is sensitive to the relativistic effect, is predicted very close to 55 meV of the experimental result [16], and also close to 57 meV of Sundholm's [12] and 55 meV of Dzuba *et al*'s [10] relativistic calculations.

Figure 1 shows photodetachment cross sections of the bound state $6s^26p\ ^2P_{3/2}$ of the negative barium atomic ion from the threshold to the 2.5 eV photon energy. Sections (a), (b) and (c) refer to three sets of partial cross sections with the total angular momentum of the final state $J = 1/2$, $3/2$ and $5/2$, respectively, and section (d) to the sum of (a), (b) and (c). The solid lines and long-dashed lines stand for the length and velocity form of the cross section, respectively. From figure 1 one can see that the partial cross section to the $J = 5/2$ symmetry contributes most to the total cross section in the region of the shown photon energy.

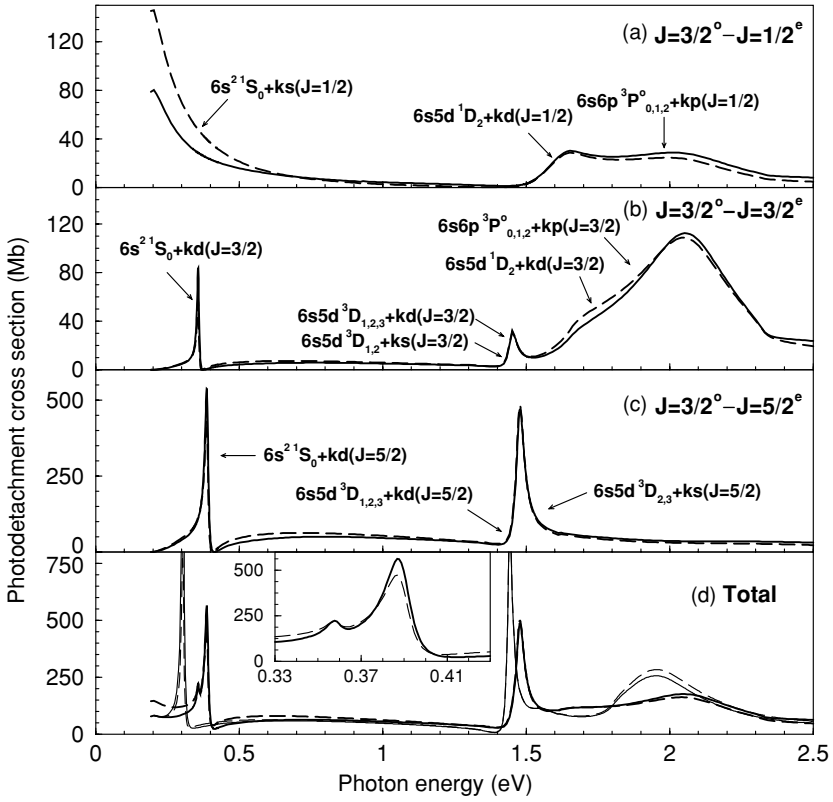

Figure 1. The partial and total photodetachment cross sections from the $6s^2 6p\ ^2P^o_{3/2}$ level of the negative atomic barium ion: (a) $J = 1/2$, (b) $J = 3/2$, (c) $J = 5/2$, and (d) the sum of (a), (b) and (c) partial cross sections. The solid lines stand for the length form of the cross section, the long-dashed lines for the velocity form. In (d), the non-relativistic R-matrix results of Yuan [39] are also shown with thin solid and dashed lines.

For convenience of discussion, we will describe the characteristics of the final states in terms of the quantum numbers of atomic energy levels and free electron orbital and the total angular momentums of the whole system. The partial cross section in figure 1(a) is mainly dominated by $[6s^2\ ^1S_0 + ks](J = 1/2)$, $[6s5d\ ^1D_2 + kd](J = 1/2)$ and $\left[6s6p\ ^3P^o_{0,1,2} + kp\right](J = 1/2)$ ionization channels. The cross section near the ionization threshold displays the typical threshold feature of the s-wave ionizing electron. From the photon energy of 1.5 eV to 2.5 eV, the structure is attributed to several broad peaks caused by a few weak shape resonances.

In figure 1(b) the ionization channels $[6s^2\ ^1S_0 + kd](J = 3/2)$, $[6s5d\ ^3D_{1,2} + ks](J = 3/2)$, $[6s5d\ ^3D_{1,2,3} + kd](J = 3/2)$, $[6s5d\ ^1D_2 + kd](J = 3/2)$ and $[6s6p\ ^3P^o_{0,1,2} + kp](J = 3/2)$ contribute to the $J = 3/2$ partial cross section. In figure 1(b) one can see two sharp peaks around 0.357 eV and 1.452 eV and a broader peak between 1.5 eV and 2.5 eV photon energy. The first sharp peak is contributed by the $[6s^2\ ^1S_0 + kd](J = 3/2)$ ionization channel with a strong $kd_{3/2}$-wave shape resonance located at 0.174 eV of the free electron energy. In the present paper, we take the position of the peak as the resonance position. This d-wave shape resonance has been studied by many authors [22–24, 39], among which the most recent non-relativistic close-coupling value of 0.122 eV [39] and an early one-channel relativistic

value of 0.220 eV are closest to the present result. The second peak lies just above the excited states 6s5d $^3D_{1,2,3}$ and is contributed by the [6s^2 $^1S_0$ + kd]($J = 3/2$), [6s5d $^3D_{1,2}$ + ks]($J = 3/2$) and [6s5d $^3D_{1,2,3}$ + kd]($J = 3/2$) ionization channels. The dominating contribution comes from the [6s5d $^3D_{1,2,3}$ + kd]($J = 3/2$) ionization channel with a mixing between $kd_{3/2}$ and $kd_{5/2}$-wave shape resonances located from 0.29 to 0.34 eV higher than the 6s5d $^3D_{1,2,3}$ excited states. The strong but broader peak between 1.5 eV and 2.5 eV is mainly caused by the $\left[6s6p\ ^3P^o_{0,1,2} + kp\right](J = 3/2)$ ionization channel. There is another structure between the second small sharp peak and the broader peak, which should be attributed to the [6s5d $^1D_2$ + kd]($J = 3/2$) ionization channel.

For the same reason as the d-wave shape resonances, figure 1(c) also shows two narrow giant shape resonances. One of them occurs at 0.388 eV photon energy, higher than the elastic threshold with a free electron energy of 0.205 eV, and the other one is located at 1.479 eV photon energy which is above the first excitation threshold. The second peak is mainly contributed by a shape resonance state of an excitation photodetachment process with the target in the excited states and the free electron with energies from 0.29 to 0.34 eV. There is a bit of difference between the widths of the two peaks, because the first peak is caused only by the [6s^2 ^{1}S + kd]($J = 5/2$) ionization channel, while the second peak is caused by the [6s5d $^3D_{2,3}$ + ks]($J = 5/2$) and [6s5d $^3D_{1,2,3}$ + kd]($J = 5/2$) ionization channels at the same time with both $kd_{3/2}$ and $kd_{5/2}$ free electrons being coupled and split due to the differences in ionization thresholds and angular momentum coupling. As the cross sections around the first resonance peaks in figures 1(b) and (c) are contributed by pure one-channel ionization, a 31 meV separation of the two peaks gives the fine-structure split of the [6s^2 ^{1}S + kd]($J = 3/2$) and [6s^2 ^{1}S + kd]($J = 5/2$) shape resonance states. The present split is about twice of the value of 15.6 meV given by Dzuba *et al* [25]. Some difference exists between the estimates of the fine-structure split. In the present case, the fine-structure split was defined as the photon energy separation between the tops of the two sharp peaks in figures 1(b) and (c), while in Dzuba *et al*'s calculation it was determined from the electron energy separation between the two $\frac{\pi}{2}$ phase shifts of the [6s^2 ^{1}S + kd]($J = 3/2$) and [6s^2 ^{1}S + kd]($J = 5/2$) scattering channels. However, at such low energies, the background of the phase shift is very small and the resonance position is almost the same as the position of the $\frac{\pi}{2}$ phase shift. Therefore, the difference in the method of determining the resonance position between the present and Dzuba *et al*'s calculations would not cause considerable uncertainties for a direct comparison. The relativistic split of the two d-wave shape resonance states is about half of the split between Ba$^-$6s^{2}6p $^2P_{1/2}$ and Ba$^-$6s^{2}6p $^2P_{3/2}$ of the attached *p*-electron. As the fine-structure split of the bound electron states has been predicted accurately by the present calculation, we believe that the fine-structure split predicted for the d-wave shape resonance is also reliable. In the calculation of Dzuba *et al*, the position of the d-wave shape resonance was at a higher energy of 0.221 eV compared to the present statistical average position 0.193 eV, so the spin-orbit interaction should be weaker for the d-wave shape resonance state in their calculations. In a later calculation, Dzuba and Gribakin [26] predicted that [6s^2 ^{1}S + kd]($J = 3/2$) has a very weak bound state at -15 meV and [6s^2 ^{1}S + kd]($J = 5/2$) has a shape resonance at 60 meV with a fine-structure split of about 75 meV. Although the authors stated that they could not prove or disprove the existence of the bound state due to the uncertainty in the calculated energy, the sensitivity of the fine-structure split depending on the position had been shown clearly. Figure 1(d) gives the total cross section from the 6s^{2}6p $^2P_{3/2}$ state. In figure 1 one can see that the length and the velocity form of the cross section agree with each other quite well. The total cross section of a non-relativistic *R*-matrix calculation is also presented in figure 1(d) for comparison. One can see that without the relativistic fine-structure splits the shape resonance peaks obtained by the non-relativistic

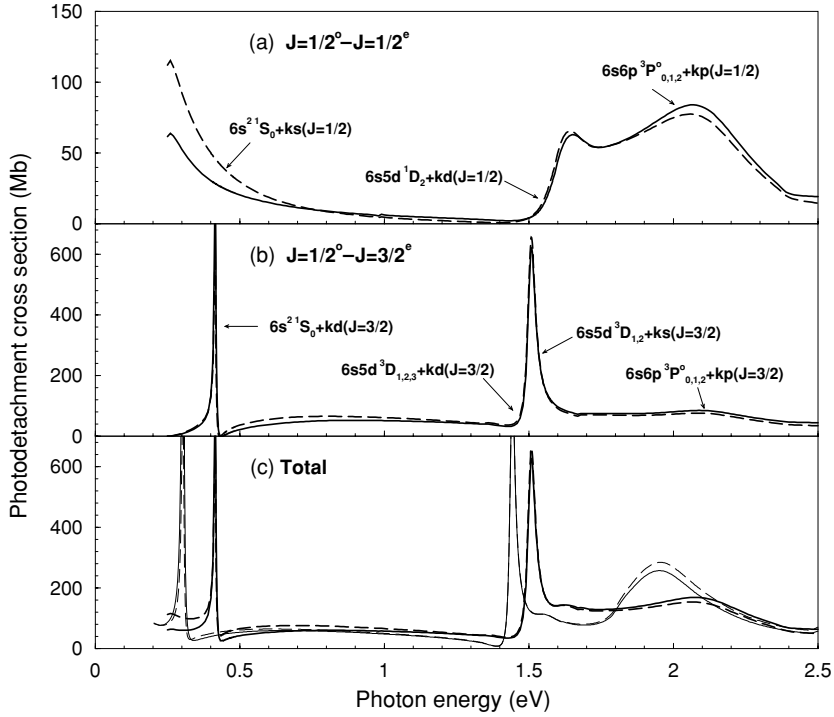

Figure 2. The partial and total photodetachment cross sections from the $6s^2 6p\ ^2P^o_{1/2}$ level of the negative atomic barium ion: (a) $J = 1/2$, (b) $J = 3/2$, and (c) the sum of (a), (b) partial cross sections. The meanings of the curves are the same as those in figure 1 and the non-relativistic R-matrix results of Yuan [39] are also shown in figure 2(c) with thin solid and dashed lines as in figure 1(d).

calculation are at a higher photon energy and more narrow than the corresponding relativistic ones.

The partial and total cross sections from the bound state $6s^2 6p\ ^2P_{1/2}$ of the negative atomic barium ion with the photon energy from threshold to 2.5 eV are illustrated in figure 2. The meanings of the curves are the same as in figure 1. In figure 2(a), the $[6s^2\ ^1S + ks](J = 1/2)$ ionizing channel gives a typical s-wave near-threshold structure at the elastic threshold. The structure between 1.5 eV to 2.5 eV is more complex. The first peak should be contributed by the $[6s5d\ ^1D_2 + kd](J = 1/2)$ ionization channel and the second one by $[6s6p\ ^3P^o_{0,1,2} + kp](J = 1/2)$. The total cross section is mainly contributed by the $J = 3/2$ partial cross section shown in figure 2(b). In figure 2(b) there are two shape resonances occurring with photon energies of 0.415 eV and 1.509 eV corresponding to a free electron energy of 0.175 eV for the first peak. The first sharp peak is contributed by the $[6s^2\ ^1S + kd](J = 3/2)$ ionizing channel while the second one is a mix structure of $[6s5d\ ^3D_{1,2} + ks](J = 3/2)$ and $[6s5d\ ^3D_{1,2,3} + kd](J = 3/2)$ ionization channels. The $\left[6s6p\ ^3P^o_{0,1,2} + kp\right](J = 3/2)$ ionization channel also contributes a broad but weak peak to the partial cross section from 1.7 eV to 2.5 eV. As with the second peak in figures 1(b) and (c), the second peak in figure 2(b) is also wider than the first one because it involves more uncertainties for the ionized electron energy and more different angular momentum coupling schemes. The agreement between the length and the velocity form is also quite good in both the partial and total cross sections shown in figure 2.

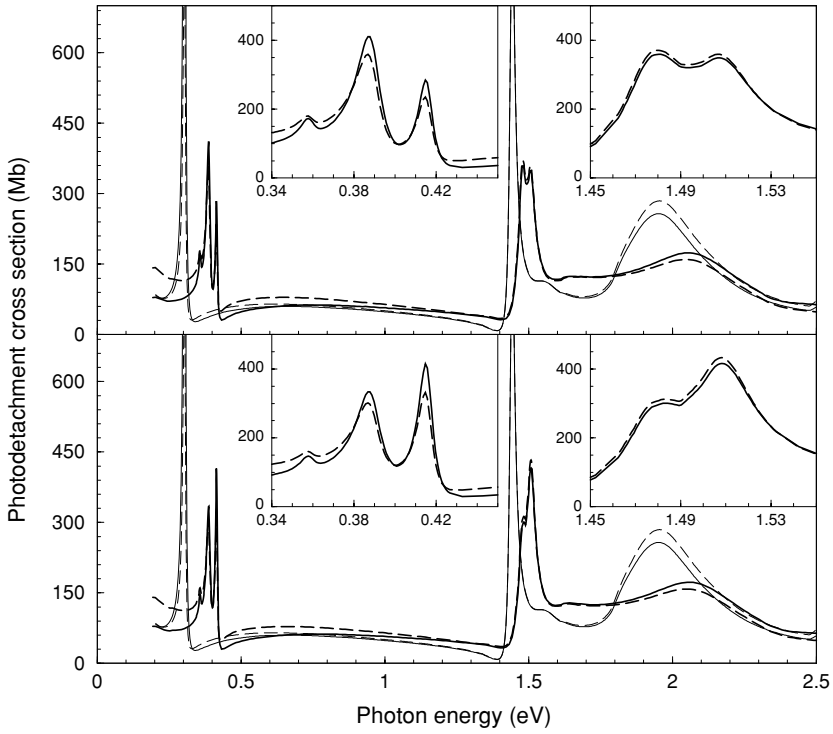

Figure 3. The total photodetachment cross sections summed over the $6s^26p\ ^2P^o_{3/2}$ and $6s^26p\ ^2P^o_{1/2}$ states of the negative atomic barium ion with their statistical weights $2J + 1$ (top) and a Boltzmann distribution among the two states at 1000 K (bottom). The meanings of the curves are the same as in figures 1 and 2 and the non-relativistic *R*-matrix results of Yuan [39] are also shown with thin lines.

In order to get the total photodetachment cross section of the negative atomic barium ion, two summations of the total cross sections from the $6s^26p\ ^2P^o_{3/2}$ and $6s^26p\ ^2P^o_{1/2}$ levels are given in figure 3. One is made according to the statistical weights $(2J + 1)$ of the two bound states and the other one is according to a Boltzmann distribution among the two states at 1000 K, which is used to simulate the barium beam temperature in experiment. One can find that the temperature has apparent influence on the detailed shapes of the fine structures around 0.4 and 1.5 eV. This is important for a quantitative comparison between theory and experiment. The solid lines and the long-dashed lines stand for the length and the velocity form of the cross section, respectively. The thick lines are the present results while the thin lines are our previous non-relativistic results. One can see that the two results are similar in general, but differences also exist between them in particular for the fine structures of the shape resonance peaks. Relativistic splits have been shown clearly for both the attached *p*-electron in the negative ion and the d-wave shape resonances. One of the most important differences is that at the two sharp peaks near the elastic and first excitation thresholds, our results predict evident relativistic effect, which can be applied in the identification of the experimental results. Another difference is that the present cross sections are smaller than our non-relativistic results where the shape resonances occur and in the photon energy range from 1.5 eV to 2.5 eV.

With the same wavefunction for the photodetachment process, the total and elastic electron scattering cross section from barium atoms are also calculated. For the convergence of the

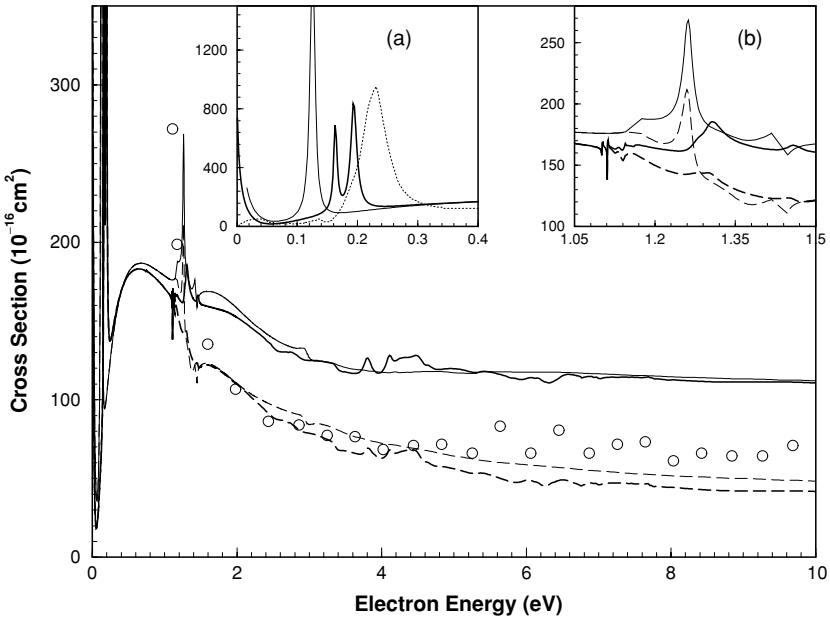

Figure 4. The total and elastic scattering cross section of an electron from barium atoms: The thick solid and long-dashed lines are the integral total and elastic cross section of the present results, while the thin lines are those of Yuan's CV results [39] and the dotted line in (a) is from Dzuba *et al* [25]. The empty circles are the experimental total integral cross sections [19].

result, we summed the contribution to the cross section of partial waves up to $J = 20\frac{1}{2}$. Figure 4 shows the integral total and elastic cross sections from threshold to 10 eV along with our early non-relativistic core–valence(CV) correlation result [39] and the experimental result [19]. Among the reported theoretical calculations of electron scattering [25–30], Fursa *et al* [29] and Adibzadeh *et al* [30] gave a wide range of total cross sections from 1 eV to 1000 eV but less attention was focused on the near threshold structure below 1 eV. Szmytkowski and Sienkiewicz [27] employed a static polarized orbital approach to approximate the dynamical process. Kelemen *et al* [28] used a local complex model potential to represent the interaction between a free electron and an atom. The uncertainties involved in their theory made it difficult to evaluate the result below 0.5 eV. Therefore, we do not plot the above four former theoretical results in the figure for comparison. In figure 4, the thick solid and long-dashed lines stand for the total and elastic cross sections of the present results respectively, while the thin lines stand for our previous results. The present results show similar structures to our previous results in general. The inset figures (a) and (b) illustrate the difference when the shape resonances occur. The non-relativistic results have two very sharp peaks at respectively 0.125 eV and 1.26 eV shown in the inset figures (a) and (b), which come from the ^2D partial wave. In inset figure (a), because of the relativistic effect we have two sharp peaks at 0.163 eV and 0.194 eV which come from $J = 3/2$ and $J = 5/2$ partial waves respectively and have typical shape resonance features. The fine-structure split of the $[6s^2\ ^1S + kd](J = 3/2)$ and $[6s^2\ ^1S + kd](J = 5/2)$ is 31 meV just as same as that we obtained in the photodetachment process. By using a relativistic many-body perturbation theory and the correction potential method, Dzuba *et al* [25] obtained total cross section from threshold to 0.04 Ry (0.544 eV). For the clarity of the figure, we only plot their results with the dotted line in the inset figure (a)

for comparison. One cannot see clearly the splitting of the d-wave resonances from their result because of the smaller fine structure interval, although the width of this resonance is very close to the present result. Also because of the relativistic effect, the present shape resonances occur at a little higher electron energy with a broader and lower resonant peak than our early non-relativistic result. For the same reason, we can explain that in the inset figure (b) the resonance distributions are also much wider than the non-relativistic result, since they come from the [6s5d $^3D_{1,2,3}$ + kd] collision channel and may split into six relativistic ionization channels. Due to overlap between ionization channels, one can not see clear splits, as shown in the inset figure (a).

The only experimental electron scattering cross sections were given by Romanyuk *et al* [19]. It is evident that there is a systematic error in their electron energy scale. With a movement of 0.8 eV of their results to higher energies, the observed threshold structure for a Sr atom at the first excited state can be moved to its actual position at 1.82 eV [39]. In figure 4, the empty circles are the integral total cross section of the experimental results [19] for Ba, which have been shifted systematically also by 0.8 eV to higher energies, as we did for the Sr atom [39]. In figure 4, we can find that both the present full relativistic and the early non-relativistic theoretical total cross sections are much higher than the experimental values for the collision energies above 1.5 eV. In our early calculations [39], after considering the core–valence electron correlation, the total cross section was about 5% lower than that of valence only, and we suspected that the discrepancy between theory and experiment was due to the relativistic effect which was not considered there. However, the present fully-relativistic calculation does not reduce the large discrepancy between theory and experiment any more. In order to clarify the source of the difference between theory and experiment, more accurate experimental measurements are needed.

In summary, we have carried out calculations on the interaction between a slow electron and barium atoms by using a fully relativistic *R*-matrix method. The results show that the total photodetachment cross section is mainly characterized by two shape resonances, above the elastic threshold and the first excitation threshold, respectively, and a broad giant structure between 1.5 eV and 2.5 eV reflecting the interactions between different ionization channels. The total electron scattering cross section from threshold to 10 eV is given. The results show that by including the relativistic effect the large discrepancy between the theoretical and experimental results still cannot be eliminated. Obvious fine-structure splits are shown compared with the corresponding non-relativistic calculations when shape resonances occur.

Acknowledgments

This work was supported by the National Science Fund for Distinguished Young Scholars under grant no 10025416, the National Natural Science Foundation of China under grant no 10474138, the National High-Tech ICF Committee in China, and China Research Association of Atomic and Molecular Data.

References

[1] Pegg D J, Thompson J S, Compton R N and Alton G D 1987 *Phys. Rev. Lett.* **59** 2267
[2] Fischer C F, Lagowski J B and Vosko S H 1987 *Phys. Rev. Lett.* **59** 2263
[3] Fischer C F 1989 *Phys. Rev.* A **39** 963
[4] Kim L and Greene C H 1989 *J. Phys. B: At. mol. Opt. Phys.* **22** L175
[5] Johnson W R, Sapirstein J and Blundell S A 1989 *J. Phys. B: At. Mol. Opt. Phys.* **22** 2341
[6] Gribakin G F, Gul'tsev B V, Ivanov V K and Kuchiev M Yu 1989 *Zh. Eksp. Teor. Fiz. Pis'ma Red.* **15** 32
[7] Fuentealba P, Savin A, Stoll H and Preuss H 1990 *Phys. Rev.* A **41** 1238

[8] Cowan R and Wilson M 1991 *Phys. Scr.* **43** 244
[9] Dzuba V, Flambuam F, Gribakin G F and Sushkov D 1991 *Phys. Rev.* A **44** 2823
[10] Dzuba V A and Gribakin G F 1997 *Phys. Rev.* A **55** 2443
[11] Van der Hart H W, Laughlin C and Hansen J E 1993 *Phys. Rev. Lett.* **71** 1506
[12] Sundholm D 1995 *J. Phys. B: At. Mol. Opt. Phys.* **28** L399
[13] Salomonson S, Warston H and Lindgren I 1996 *Phys. Rev. Lett.* **76** 3092
[14] Nadeau M-J, Zhao X-L, Garwan M and Litherland A 1992 *Phys. Rev.* A **46** R3588
[15] Petrunin V V, Andersen H H, Balling P and Anderson T 1996 *Phys. Rev. Lett.* **76** 744
[16] Petrumin V V, Voldstad J D, Balling P, Kristensen P, Anderson T and Haugen H K 1995 *Phys. Rev. Lett.* **75** 1911
[17] Fabrikant I I 1975 *Atomniye Protsessi* (Riga: Zinatne) p 80
[18] Fabrikant I I 1988 *Phys. Rep.* **159** 1
[19] Romanyuk N I, Shpenik O B and Zapesochyi I P 1980 *Pis'ma Zh. Eksp. Teor. Fiz.* **32** 472
[20] Kurtz H A and Jordan K D 1981 *J. Phys. B: At. Mol. Opt. Phys.* **14** 4361
[21] Amusia M Ya, Sosnivker V A, Cherepkov N A and Chernysheva L V 1985 *Zh. Tekh. Fiz.* **55** 2304
[22] Yuan J and Zhang Z 1989 *J. Phys. B: At. Mol. Opt. Phys.* **22** 2751
Yuan J and Zhang Z 1990 *Phys. Rev.* A **42** 5363
Yuan J 1995 *Phys. Rev.* A **52** 4647
[23] Johnston A R, Gallup G A and Burrow P D 1989 *Phys. Rev.* A **40** 4770
[24] Gribakin G F, Gul'tsev B V, Ivanov V K, Kuchiev M Yu and Tančić A R 1992 *Phys. Lett.* A **164** 73
[25] Dzuba V A, Flambaum V V and Suchkov O P 1991 *Phys. Rev.* A **44** 4224
[26] Dzuba V A and Gribakin G F 1994 *Phys. Rev.* A **49** 2483
[27] Szmytkowski R and Sienkiewicz J E 1994 *Phys. Rev.* A **50** 4007
[28] Kelemen V I, Remeta E Yu and Sabad E P 1995 *J. Phys. B: At. Mol. Opt. Phys.* **28** 1527
[29] Fursa D V and Bray I 1999 *Phys. Rev.* A **59** 282
[30] Adibzadeh M and Theodosiou C E 2004 *Phys. Rev.* A **70** 052704
[31] Heinicke E, Kaiser H J, Rackwits R and Feldmann D 1974 *Phys. Lett.* A **50** 265
[32] Walter C W and Peterson J R 1992 *Phys. Rev. Lett.* **68** 2281
Peterson J R 1992 *Aust. J. Phys.* **40** 293
[33] Kristensen P, Brodie C A, Pedersen U V, Petrunin V V and Andersen T 1997 *Phys. Rev. Lett.* **78** 2329
[34] Lee D H, Pegg D J and Hanstorp D 1998 *Phys. Rev.* A **58** 2121
[35] Gribakin G F, Gul'tsev B V, Ivanov V K and Kuchiev M Yu 1990 *J. Phys. B: At. Mol. Opt. Phys.* **23** 4505
[36] Fischer C F and Hansen J E 1991 *Phys. Rev.* A **44** 1559
[37] Yuan J and Fritsche L 1997 *Phys. Rev.* A **55** 1020
Yuan J 2000 *Phys. Rev.* A **61** 012704
[38] Yuan J and Lin C D 1998 *Phys. Rev.* A **58** 2824
[39] Yuan J 2003 *J. Phys. B: At. Mol. Opt. Phys.* **36** 2053
[40] Burke P G, Hibbert A and Robb W D 1971 *J. Phys. B: At. Mol. Opt. Phys.* **4** 153
[41] Norrington P H and Grant I P 1987 *J. Phys. B: At. Mol. Opt. Phys.* **20** 4869
[42] Wijesundera W P, Parpia F A, Grant I P and Norrington P H 1991 *J. Phys. B: At. Mol. Opt. Phys.* **24** 1803
[43] Dyall K G, Grant I P, Johnson C T, Parpia F A and Plummer E P 1989 *Comput. Phys. Commun.* **55** 425
[44] Moore C E (ed) 1970 *Atomic Energy Levels (NBS Title Series No 3)* (Washington, DC: US Government Printing Office) p 131